Effects of Postannealing Process on the Properties of RuO2 Films and Their Performance As Electrodes in Organic Thin Film Transistors or Solar Cells

9 AUTHORS, INCLUDING:

Sae Byeok Jo
University of Washington Seattle
28 PUBLICATIONS **440** CITATIONS

SEE PROFILE

Ji-Wook Jang
Helmholtz-Zentrum Berlin
52 PUBLICATIONS **1,183** CITATIONS

SEE PROFILE

Shi-Woo Rhee
Pohang University of Science and Technology
231 PUBLICATIONS **3,490** CITATIONS

SEE PROFILE

Effects of Postannealing Process on the Properties of RuO$_2$ Films and Their Performance As Electrodes in Organic Thin Film Transistors or Solar Cells

Dong-Jin Yun,*,[†] Hye-min Ra,[‡] Sae Byeok Jo,[‡] Wanjoo Maeng,[†] Seung-hyup Lee,[†] Sunghoon Park,[†] Ji-Wook Jang,[‡] Kilwon Cho,[‡] and Shi-Woo Rhee*,[‡]

[†]Samsung Advanced Institute of Technology, Suwon 440-600, Republic of Korea

[‡]Department of Chemical Engineering of Pohang University of Science and Technology (POSTECH), Pohang 790-784, Republic of Korea

ABSTRACT: RuO$_2$ films were deposited on SiO$_2$ (300 nm)/ N++Si substrates using radio frequency magnetron sputtering at room temperature. As-deposited RuO$_2$ films were annealed at different temperatures (100, 300, and 500 °C) and ambients (Ar, O$_2$ and vacuum), and the resulting effects on the electrical and physical properties of RuO$_2$ films were characterized. The effect of annealing atmosphere was negligible, however the temperature highly influenced the resistivity and crystallinity of RuO$_2$ films. RuO$_2$ films annealed at high temperature exhibited lower resistivity and higher crystallinity than as-deposited RuO$_2$. To investigate the possibility to use RuO$_2$ film as alternative electrodes in flexible devices, as-deposited and annealed

RuO$_2$ films were applied as the source/drain (S/D) electrodes in organic thin film transistor (OTFT), catalytic electrodes in dye sensitized solar cell (DSSC) and as the hole-injection buffer layer (HIL) in organic photovoltaic (OPV). Except for OTFTs ($\mu \approx 0.45$ cm^2/(V s) and on/off ratio $\approx 5\times 10^5$) with RuO$_2$ S/D electrodes, the DSSC and OPV (3.5% and 2.56%) incorporating annealed RuO$_2$ electrodes showed higher performance than those with as-deposited RuO$_2$ electrodes (3.0% and 1.61%, respectively).

KEYWORDS: pentacene thin film transistor, annealing process, ruthenium oxide, work-function, dye sensitized solar cell, organic photovoltaic
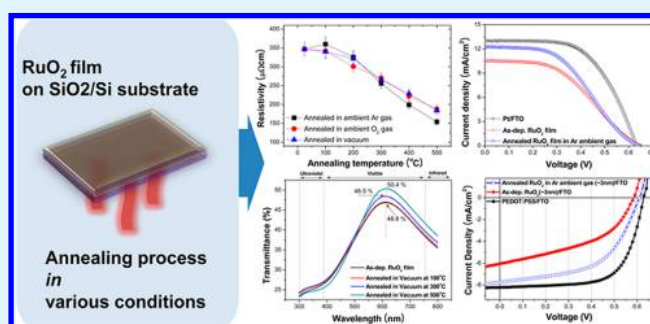
■ INTRODUCTION

Ruthenium oxide (RuO$_2$) is an attractive candidate for source and drain (S/D) electrodes in organic thin film transistors (OTFT) owing to their high work-function ($\sim$5.0 eV).[1−3] Recently, our group characterized RuO$_2$ film, which have been mainly used as buffer layers in organic light emitting device (OLED) and silicon devices, as S/D electrodes in OTFTs, and the corresponding devices exhibited higher performance than those using gold (Au) S/D electrodes.[1,2] Nevertheless, the electrical resistivity of RuO$_2$ film is still relatively high to replace metallic electrode, such as gold, platinum, or copper electrodes in industry.

In general, thermal annealing processes are utilized with the purpose of modifying the surface or bulk properties of thin films. Even though intrinsic material properties are usually retained, the properties of thin films including crystallinity, bonding states and work-function highly depend on their process conditions.[4−6] Therefore, it is anticipated that thermal treatment of RuO$_2$ films can be an efficient way to enhance their electrical conductivity.

RuO$_2$ films have a high potential to be applied in various fields, such as S/D electrodes in OTFT devices because of the high work-function, conductivity, and catalytic activity.[2,3,7,8] The hole injection buffer layer (HIL) at the organic semiconductor/cathode electrode interface in organic photovoltaics (OPV) and the catalyst counter electrode (CCE) of dye sensitized solar cells (DSSC) are good examples of RuO$_2$ applications, because the buffer layer at organic semiconductor/cathode interfaces and CCE of DSSC require high work-function[9−11] and catalytic activity[12−14] for prompt electron/hole transport at semiconductor/cathode or electrolyte/cathode interfaces, respectively. However, the applications of RuO$_2$ films as the buffer layer of OPV or CCE of DSSC have not been studied intensively despite their excellent electrical properties, while the alternative materials for buffer layers in OPV and CCE of DSSC have been needed for years due to high cost, corrosion or stability problems of conventional buffer layer (poly(3,4-ethylene dioxythiophene)/ poly(styrene sulfonate), PEDOT:PSS) and CCE (Platinum) of DSSC.
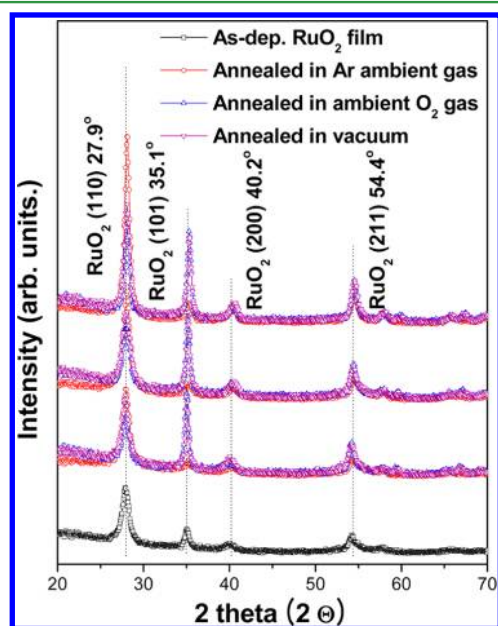
In this work, a radio frequency (r.f.) magnetron sputtering system is used to deposit RuO_2 film using a Ru metal target, and the effects of postannealing processes on the properties of RuO_2 films such as resistivity, crystallinity, work-function and bonding states are characterized. On the basis of above results, as-deposited (as-deposited) and annealed RuO_2 films are applied as S/D electrodes in pentacene TFTs, buffer layers on cathode electrode of OPV and CCE of DSSC, and the associated device performances are examined.

■ EXPERIMENTAL SECTION

RuO_2 films (thickness = 50 nm) were deposited on SiO2 (300 nm)/N++Si substrates using r.f. magnetron sputtering with a Ru metal target (2 in. diameter, 99.9%), and the gas flow ratio and sputtering power were fixed at (Ar/O_2 = 25: 25) and 50 W, respectively. The base pressure of the deposition chamber was maintained at 2×10^{-5} Torr and the working pressure was 7×10^{-3} Torr. RuO_2 films were annealed using a furnace at different temperatures (100, 300, and 500 °C) and different ambient gas conditions (Ar and O_2 gas at 1 Torr) and in vacuum (<0.01 Torr) each for 1 h.

Pentacene TFTs, DSSCs and OPVs with as-deposited and annealed RuO_2 films were fabricated to characterize and compare the performance of as-deposited and annealed RuO_2 films as S/D electrodes in pentacene TFT, CCE of DSSC, and buffer layer on cathode electrode of OPV, respectively. The detailed experimental procedures, which were applied to the fabrication of pentacene TFTs, DSSCs, and OPV, are summarized in former publications.[2,3,10,15,16]

The resistivities and morphologies of RuO_2 films were measured with the 4-point probe method (KEITHLEY 2400 sourcemeter) and atomic force measurement (AFM, veeco nanoscope in NCNT). The crystallinity and optical transmittance of RuO_2 films were investigated by X-ray diffraction (XRD, modified Philips-1880 diffractometer) and UV−vis-spectrophotometry. X-ray and ultraviolet photoemission spectroscopy (XPS and UPS, ESCALAB) were used to analyze the bonding states and work-functions of RuO_2 films. The current−voltage (I−V) characteristics of pentacene TFT and solar cells (DSSC and OPV) were measured at room temperature using an Agilent E5270A precision semiconductor parameter analyzer and solar simulator equipped with

a source meter (Keithley 2400) and a 300 W xenon lamp (AM 1.5, 100 mW/cm²), respectively.
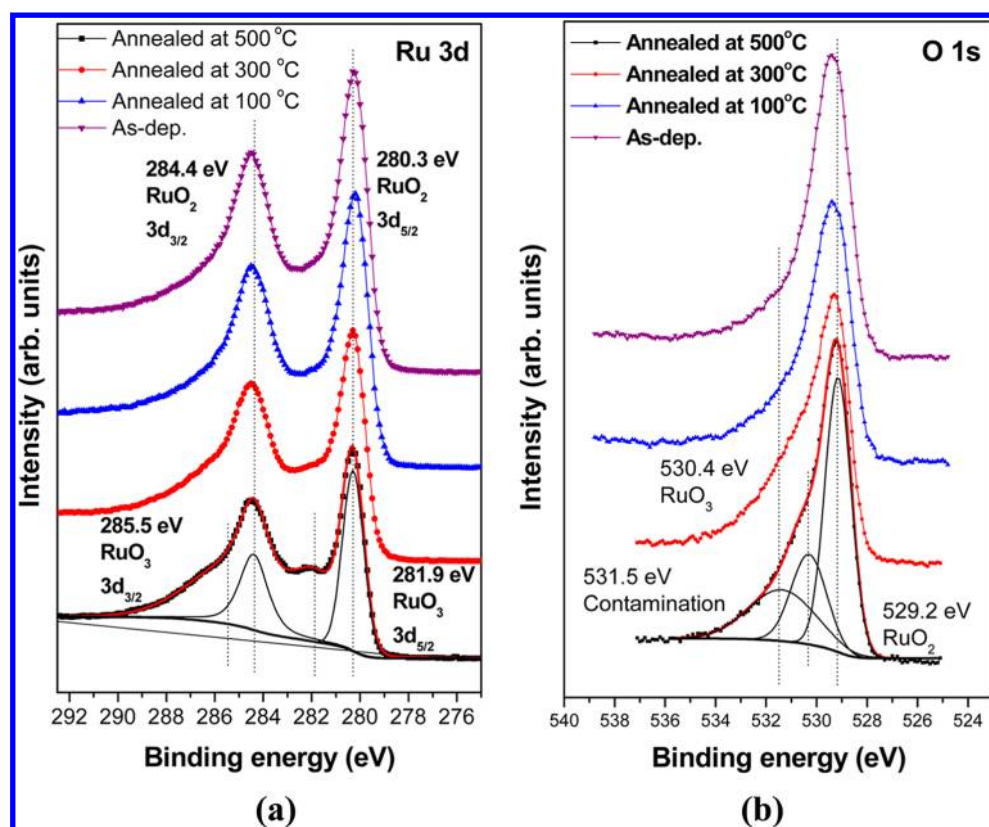
■ RESULTS AND DISCUSSION

The crystallinity of as-deposited and annealed RuO_2 films, were characterized by XRD measurement, as shown in Figure 1. The XRD pattern of as-deposited RuO_2 film consists of a (110) main peak, (101), (200), and (211) small peaks, which clearly correspond to RuO_2. After annealing the RuO_2 film, the intensities of the RuO_2 XRD peaks indicating films increase as a function of annealing temperature but there is no significant phase change.[3,17] On the other hand, RuO_2 films annealed in different atmospheres all result in similar XRD patterns. Thus, it may be deduced that the annealing ambient has negligible effects on the film microstructure and the crystallinity improvement after the annealing process is mainly attributed to the removal of lattice misfits and crystal defects by a thermally assisted mechanism.

Figure 2a shows the AFM images of as-deposited and annealed RuO_2 films. In a way similar to the XRD patterns of annealed RuO_2 films, as annealing temperature increases, the surface
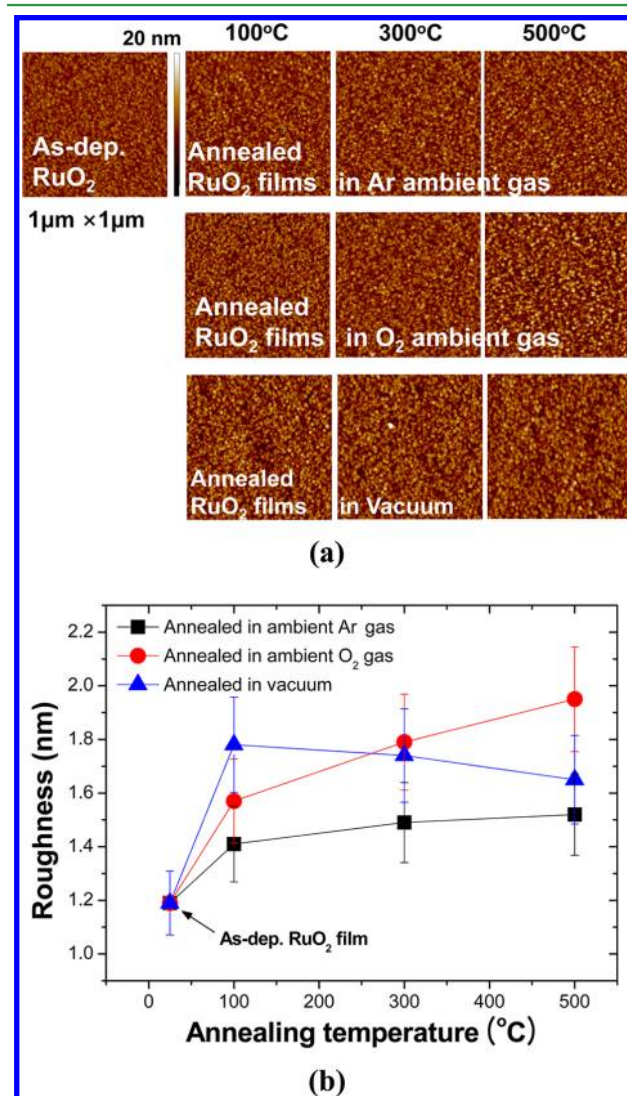
Figure 2. AFM images (1 μm × 1 μm) of as-deposited and annealed RuO_2 films and surface roughness change of RuO_2 films as a function of annealing temperature.

Figure 1. Comparative XRD patterns of as-deposited and annealed RuO_2 films, which were annealed at different temperatures and ambient gas conditions.

Figure 3. Comparative (a) Ru 3d and (b) O 1s core levels of as-deposited and annealed RuO_2 films in O_2 ambient gas at various annealing temperatures (100, 300, and 500 °C).

roughness and grain size of RuO_2 films slightly increase (<1 nm) but the annealing ambient has no significant effect on the morphology, as summarized in Figure 2b.

The Ru 3d and O 1s core-levels of as-deposited and annealed RuO_2 films were investigated by XPS measurement, as shown in Figure 3a and b. On the basis of the XPS spectra of Ru 3d and O 1s core levels, the annealing temperature and ambient gas condition of annealing process has little effect on the bonding states of RuO_2 films. The Ru 3d and O 1s XPS spectra of as-deposited and annealed RuO_2 films mainly consist of the RuO_2 peaks (Ru $3d_{3/2}$, 284.4 eV; Ru $3d_{5/2}$, 280.3 eV; O 1s, 529.2 eV), and their relative intensities is preserved even after the annealing process.[2,17] Compared to the RuO_2 films annealed in Ar gas and vacuum, the RuO_2 films annealed in O_2 atmosphere exhibit the RuO_3 bonding state and the peaks such a state become more intense as the annealing temperature increases. It seems that the formation of RuO_3 bonding originates from the diffusion of highly reactive oxygen gas into RuO_2 film at high temperature.[18,19]
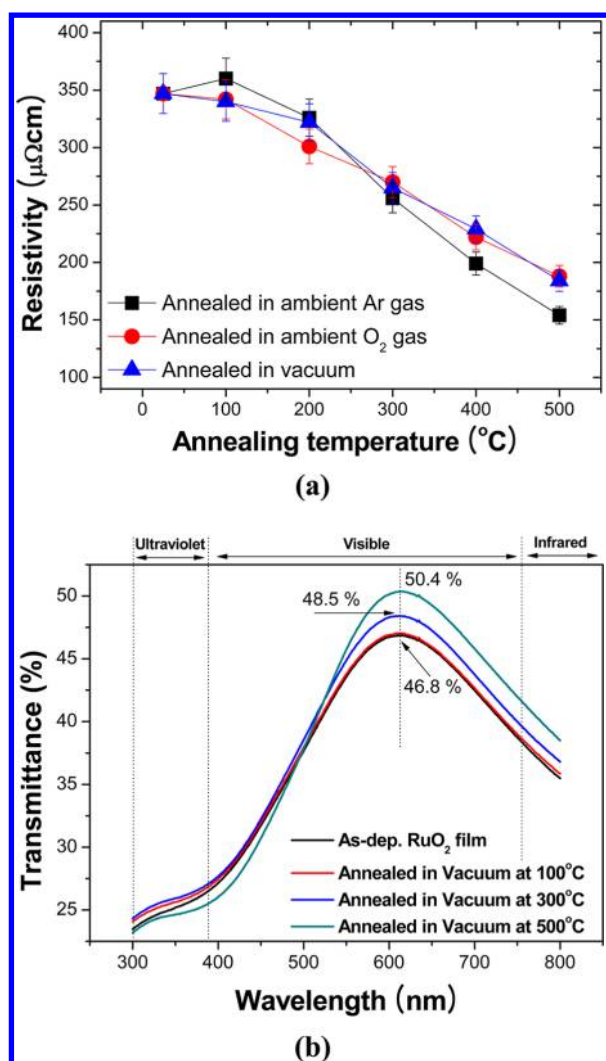
The resistivity and transmittance changes of RuO_2 films as a function of annealing temperature are shown in Figure 4a and b, respectively. As annealing temperature increases, the resistivity values of RuO_2 films gradually decreased. Independent of ambient gas condition, the RuO_2 films annealed at 100 °C have similar resistivity values near 350 ± 20 $\mu\Omega$cm, which are not distinguished from the resistivity of as-deposited RuO_2 film (347 ± 17 $\mu\Omega$cm). However, the resistivities of RuO_2 films annealed at above 200 °C are lower than those of as-deposited RuO_2 films and further decreased further with increased annealing temperature. Independent of ambient gas condition, the resistivities of RuO_2 films annealed at a fixed annealing temperature

were similar values and the resistivities of RuO_2 films annealed at 300, 400, and 500 °C were approximately 260, 210, and 170 $\mu\Omega$cm, respectively. On the other hand, the transmittance of RuO_2 film was also affected by annealing process in the visible wavelength region as shown in Figure 4b. The transmittance of as-deposited and annealed RuO_2 films (in a vacuum state) are typically compared in Figure 4b, and the transmittance-change of RuO_2 film after annealing was also independent of ambient gas just like other properties such as resistivity, morphology and crystallinity. Both resistivity and transmittance changes may be attributed to crystallinity improvement after the annealing process. It is suspected that the crystallinity improvement reduces light scattering or charge-carrier tapping so that conductivity and transmittance of RuO_2 film could increase.[20]

UPS measurements of as-deposited and annealed RuO_2 films were performed to analyze the effect of annealing process on the work-function of RuO_2 film. The work-functions of RuO_2 films were calculated using the following eq 1.[2,3]

$$\phi_M = h\nu(= 21.2 \text{ eV}) - E_{\text{cutoff(metal)}} + E_{\text{Fermi(metal)}} \quad (1)$$

Here, $h\nu$ (=21.2 eV), $E_{\text{cutoff(metal)}}$, and $E_{\text{Fermi(metal)}}$ are incoming photon energy from He I source, secondary cutoff energy of RuO_2 film, and Fermi energy of RuO_2 film, respectively. From eq 1 and the UPS spectra in Figure 5, the work-functions of as-deposited and annealed RuO_2 films were calculated, and as-deposited RuO_2 film showed a work-function value near ~5.2 eV. The work-function of the RuO_2 film slightly decreased after annealing. Regardless of the ambient gas condition (O_2 ambient, Ar ambient or vacuum), the work-functions of RuO_2 films annealed at 300 °C showed 5.17 eV $\pm$ 0.05, which are similar values to that of as-deposited RuO_2 film, but the work-functions

Figure 4. (a) Resistivity and (b) transmitance changes of annealed RuO_2 films in vacuum as a function of annealing temperature.

where I_{DS} is the drain current at a specific gate voltage (V_G), W the channel width, L the channel length, V_T the threshold voltage, μ the carrier field effect mobility and C_i the capacitance per unit area of the gate insulator (C_i of 300 nm thick SiO_2 was measured to be 10 nF/cm^2). Figure 6 (b) shows the transfer curves of pentacene TFTs with RuO_2 S/D electrodes, which were measured in the backward direction from 20 V to −40 V. The on/off ratio and μ of pentacene TFT were not improved after annealing of the S/D electrodes but the values were comparable to or higher than those of pentacene TFTs with Au S/D electrodes (on/off ratio = 10^6 and μ = 0.28 cm^2/(V s)).[2,3] The μ and on/off ratio of pentacene TFTs with RuO_2 S/D electrode annealed at 300 °C and N_2 ambient gas condition were ~0.45 cm^2/(V s) and ~5 × 10^5, which are almost identical to those of performance with pentacene TFTs with as-deposited RuO_2 S/D electrodes. The pentacene TFT with RuO_2 S/D electrode annealed at 300 °C and N_2 ambient gas condition also showed almost the same output curve to that with as-deposited RuO_2 S/D electrode, as shown in Figure 5c. The resistivity-decrease of RuO_2 S/D electrodes after annealing did not significantly affect to the electrical properties of pentacene TFTs because of the short channel length of the pentacene TFT and the sufficient conductivity of as-deposited RuO_2 S/D film. On the other hand, in the case of pentacene TFT with RuO_2 S/D electrodes annealed at 500 °C, μ and on/off ratio unexpectedly degraded to ~0.2 cm^2/(V s) and ~10^5 and a hysteresis behavior in the transfer characteristics appeared, as shown in Figure 5b and d. We believe that the performance deterioration of pentacene TFTs originated from the thermal damage of OTS monolayers on the dielectrics after the annealing process. The degradation of OTS monolayers on the gate dielectric induces trap sites near the channel region that hinder transfer of hole carriers in the channel.

The resistivity improvement of RuO_2 films after annealing did not affect the performance of S/D electrodes, but highly improved the performance of large-area electrodes in solar cells. Because RuO_2 has high catalytic activity and conductivity, it is expected that RuO_2 film can be utilized as a catalytic counter electrode between the electrolyte and the conductive counter electrode. The performance of DSSCs with RuO_2 CCE (50 nm) were characterized with a solar simulator under one sun illumination. The $I-V$ curves are shown in Figure 7a and the solar cell parameters including short-circuit current density (J_{sc}), open circuit voltage (V_{oc}), fill factor (FF), and efficiency (η) are summarized in Table 1. The DSSC with as-deposited RuO_2 CCE showed J_{sc} of 10.5 mAcm^{-2}, FF of 43%, and efficiency of 3.0%, and these results confirmed that the potential use of as-deposited RuO_2 film as a CCE of DSSC, even though the performance of DSSC with RuO_2 film is somewhat inferior to that of Pt CCE (J_{sc} = 13.0 mAcm^{-2}, FF = 0.58, and η = 4.8%). The J_{sc}, FF, and efficiency of DSSC with RuO_2 CCE were further improved up to J_{sc} = 12.2 mAcm^{-2}, FF = 45%, and η = 3.5% because of the high conductivity of RuO_2 CCE annealed at 500 °C.

On the other hand, a potential application of RuO_2 film consists of the HIL between P3HT:PCBM active layer and conducting transparent anode is owing to high work-function (~5.0 eV) and conductivity of RuO_2. The HIL that has a high work-function has the role of reducing the interface resistance during the hole-extraction process from the active layer to the anode. As studied by UPS analysis, RuO_2 film has a high work-function (~ 5.0 eV) comparable to that of PEDOT:PSS films (4.9−5.0 eV), which are commonly used as a hole injection layer, and moreover the conductivity of RuO_2 film is much higher than

of RuO_2 film decreased to ~5.03 eV after annealing process at 500 °C. The work-function change of RuO_2 film is highly related to the crystallinity improvement of RuO_2 film at annealing process. After annealing at high temperature, the crystal defect or lattice misfits at the RuO_2 film surface are suspected to decrease so that the electron density of RuO_2 film at surface region could be increased. As a result, the work-functions of the RuO_2 films slightly decreases after annealing.[20]

OTFTs, DSSCs, and OPVs with as-deposited and annealed RuO_2 electrodes were fabricated and characterized to investigate the possible use of RuO_2 films as electrodes for organic electronics and the effects of annealing process on the electrode performance.
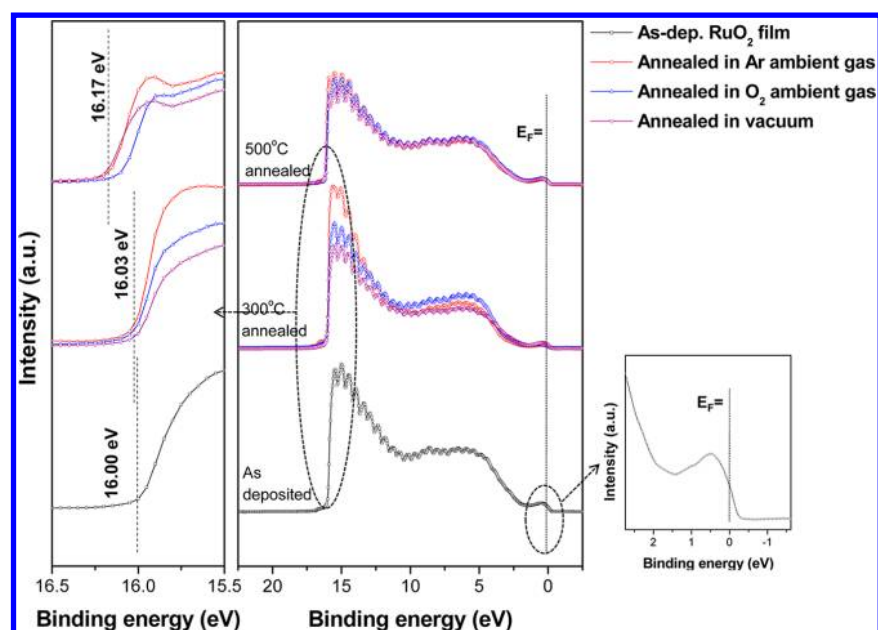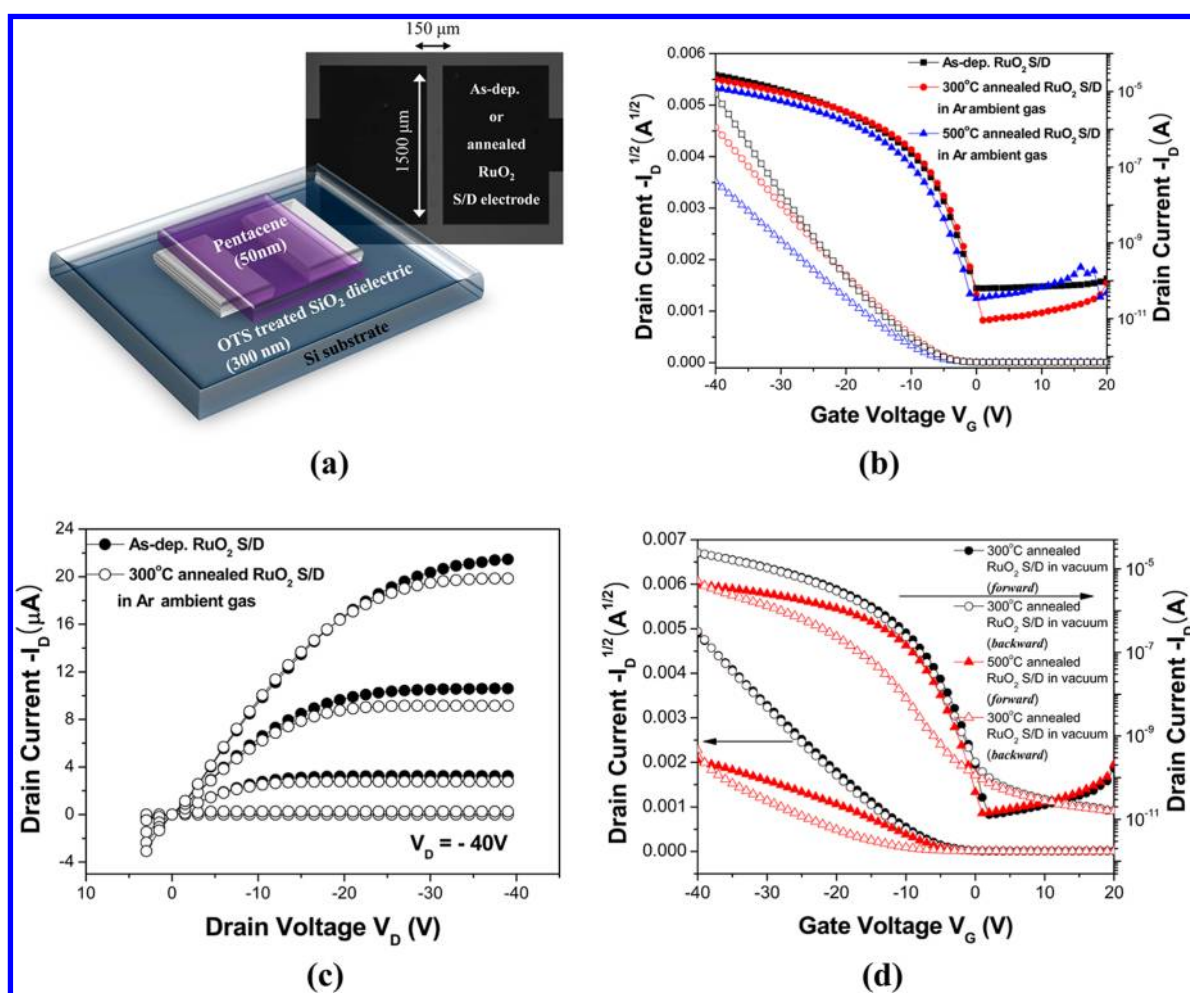
Bottom-contact pentacene TFTs were fabricated using as-deposited and annealed RuO_2 films as S/D electrodes, as shown Figure 6a. After patterning of the S/D electrodes, annealing was performed and pentacene semiconductor was deposited. The $I-V$ characteristic of the pentacene TFT with as-deposited and annealed RuO_2 S/D electrodes were studied. The field-effect mobility in the saturation regime (V_D = −40 V) was calculated using the formula given below:[2,3]

$$I_{DS} = \frac{WC_i}{2L}(V_G - V_T)^2 \mu \qquad (2)$$

4591

dx.doi.org/10.1021/am300949h | *ACS Appl. Mater. Interfaces* 2012, 4, 4588−4594
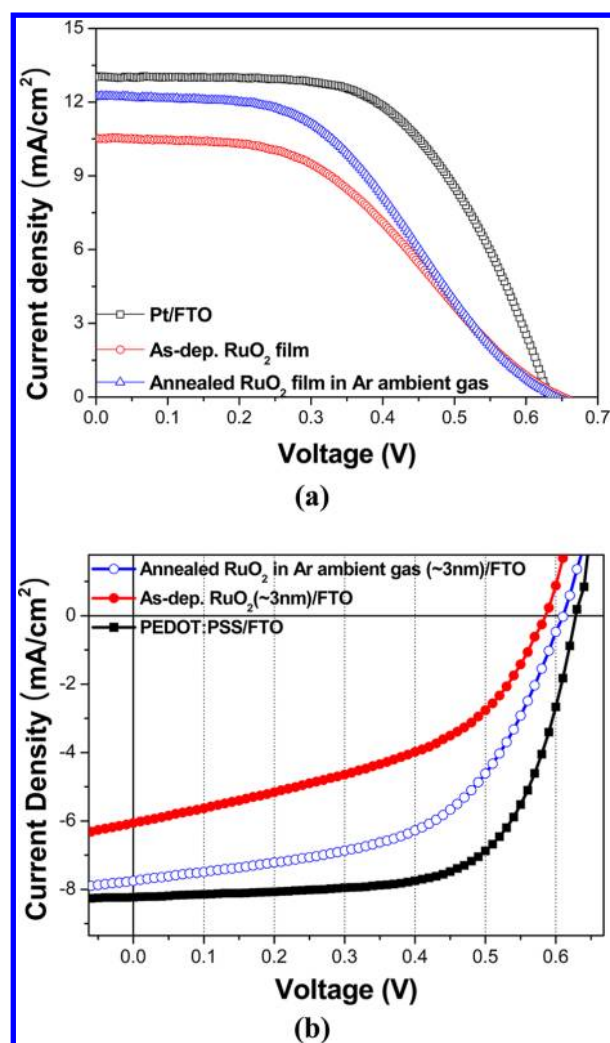
Figure 5. Comparative UPS spectra including Secondary cutoff and Fermi edge regions of as-deposited and annealed RuO_2 films under various conditions.

Figure 6. (a) Schematic diagram of a bottom-contact pentacene TFT with S/D electrode, comparative (b) transfer and (c) output characteristics of pentacene TFTs with as-deposited and annealed RuO_2 S/D electrodes, and (d) current−voltage hysteresis of pentacene TFTs with RuO_2 S/D electrodes annealed at 300 and 500 °C.

Figure 7. Comparative $I{-}V$ characteristics of (a) DSSC and (b) OPV with RuO$_2$ and reference electrodes.

CONCLUSIONS

RuO$_2$ films deposited by r.f. sputtering were annealed at various conditions and the property variations of RuO$_2$ films depending on annealing condition were clearly characterized. There is no significant effect of ambient gas during the annealing process on the properties of RuO$_2$ film, but higher annealing temperatures resulted in lower resistivity values. The resistivity reduction after the annealing process did not improve the performance of RuO$_2$ films as S/D electrodes of organic thin film transistors but highly improved the catalytic performance as an electrode in OPV. Therefore, RuO$_2$ material is a strong alternative candidate for replacing expensive common electrodes in organic electronics.

AUTHOR INFORMATION

Corresponding Author
*E-mail: DongJin.Yun@samsung.com (D.-J.Y.); Srhee@postech.ac.kr (S.-W.R.). Tel: 82-54-275-2265. Fax: 82-54-2798619.

Notes
The authors declare no competing financial interest.

ACKNOWLEDGMENTS

REFERENCES

(1) Kim, S. W.; Baik, J. M.; Lee, J. L. *Electrochem. Solid-State Lett.* **2005**, *8*, H79.
(2) Yun, D. J.; Rhee, S. W. *J. Mater. Chem.* **2005**, *20*, 9754.
(3) Yun, D. J.; Lee, S.; Yong, K.; Rhee, S. W. *Appl. Phys. Lett.* **2010**, *97*, 073303.
(4) Kim, W. G.; Rhee, S. W. *Microelectron. Eng.* **2009**, *86*, 2153.
(5) Yun, D. J.; Rhee, S. W. *Org. Electron.* **2008**, *9*, 551.
(6) Chang, J. F.; Lin, W. C.; Hon, M. H. *Appl. Surf. Sci.* **2001**, *183*, 18.
(7) Rolison, D. R.; Hagans, P. L.; Swider, K. E.; Long, J. W. *Langmuir* **1999**, *15*, 774.
(8) Ma, H.; Liu, C.; Liao, J.; Su, Y.; Xue, X.; Xing, W. *J. Mol. Catal. A: Chem.* **2006**, *247*, 7.
(9) Girotto, C.; Voroshazi, E.; Cheynst, D.; Heremans, P.; Rand, B. P. *ACS Appl. Mater. Interfaces* **2011**, *3*, 3244.
(10) Kim, J. S.; Park, J. H.; Lee, J. H.; Jo, J.; Kim, D. Y.; Cho, K. *Appl. Phys. Lett.* **2007**, *91*, 112111.
(11) Choulis, S. A.; Choong, V. E.; Patwardhan, A.; Mathai, M. K.; So, F. *Adv. Func. Mater.* **2006**, *16*, 1075.
(12) Fang, X.; Ma, T.; Guan, G.; Akiyama, M.; Kida, T.; Abe, E. *J. Electrochem. Soc.* **2004**, *570*, 257.
(13) Suzuki, K.; Yamaguchi, M.; Kumagai, M.; Yanagida, S. *Chem. Lett.* **2003**, *32*, 28.

conducting polymers including PEDOT:PSS. The $I{-}V$ characteristics of OPVs with different buffer layers (PEDOT:PSS and RuO$_2$ thin films) are shown in Figure 7b. As shown in Figure 6 and Table 1, the photoelectronic conversion efficiency of an OPV cell with as-deposited RuO$_2$ buffer layer was 1.61%, which value is much poorer than that of OPV with PEDOT:PSS buffer layer (3.45%) because of low J_{sc} (6.06 mA/cm^2). After annealing the RuO$_2$ buffer layer, the hole transport between active layer and conducting transparent anode was improved owing to the conductivity enhancement of the RuO$_2$ buffer layer, and thus the J_{sc} (7.75 mA/cm^2) and η (2.56%) of OPV with RuO$_2$ buffer layer are shown to approach the performance of OPV cells with a PEDOT:PSS buffer layer (J_{sc}: 8.23 mA/cm^2 and η: 3.45%).

Table 1. Photoelectronic Characteristics of DSSC and OPVs with RuO$_2$ and Reference Electrodes

device type	electrode	V_{OC} (mV)	J_{SC} (mA cm^{-2})	FF (%)	H (%)
DSSC	Pt/FTO	633.1 ± 0.5	13.0 ± 0.2	58 ± 0.5	4.8 ± 0.5
	as-deposited RuO$_2$ (50 nm)/FTO	651.2 ± 0.5	10.5 ± 0.2	43 ± 0.5	3.0 ± 0.5
	annealed RuO$_2$/FTO in Ar ambient gas	639.1 ± 0.5	12.2 ± 0.2	45 ± 0.5	3.5 ± 0.5
OPV	PEDOT:PSS/FTO	630 ± 0.5	8.23 ± 0.2	63 ± 0.2	3.45 ± 0.2
	as-deposited RuO$_2$ (~3 nm)/FTO	590 ± 0.5	6.06 ± 0.2	59 ± 0.2	1.61 ± 0.2
	annealed RuO$_2$/FTO in Ar ambient gas	610 ± 0.5	7.75 ± 0.2	61 ± 0.2	2.56 ± 0.2

(14) Murakami, T. N.; Gratzel, M. *Inorg. Chim. Acta* **2008**, *361*, 572.

(15) Ganapathy, V.; Karunagaran, B.; Rhee, S. W. *J. Power Sources* **2010**, *195*, 5138.

(16) Jo, S. B.; Lee, J. H.; Sim, M.; Kim, M.; Park, J. H.; Choi, Y. S.; Kim, Y.; Ihn, S. G.; Cho, K. *Adv. Funct. Mater.* **2011**, *1*, 690.

(17) Lee, D. J.; Kang, S. W.; Rhee, S. W. *Thin Solid Films* **2002**, *413*, 237.

(18) Subhramannia, M.; Balan, B. K.; Sathe, B. R.; Mulla, I. S.; Pillai, V. K. *J. Phys. Chem. C* **2007**, *111*, 16593.

(19) Kim, Y. J.; Gao, Y.; Chambers, S. A. *Appl. Surf. Sci.* **1997**, *120*, 250.

(20) Vayunandana Reddy, Y. K.; Mergel, D. *J. Mater. Sci.* **2006**, *17*, 1029.